Supporting Information

The synergetic effect for mixed-phase of NiMoO$_4$ with 1D–2D–3D hierarchical structure for highly efficient and stable urea oxidation reaction

Yao Zhang [a, b], Haoran Guo [a], Xinpan Li [c], Wenlu Ren [a], and Rui Song*[a]

[a] School of Chemical Sciences, University of Chinese Academy of Sciences, 19 Yuquan Road, Shijingshan District, Beijing, 100049, PR China

[b] School of Materials and Chemical Engineering, Xuzhou University of Technology, Xuzhou 221018, PR China

[c] Institute of Chemistry, Chinese Academy of Sciences (CAS), 2 Zhongguancun North Road, Haidian District, Beijing, 100190, PR China

*Email: rsong@ucas.ac.cn

Experimental Section

Chemicals and Reagents

Sodium molybdate dihydrate ($Na_2MoO_4 \cdot 2H_2O$), iridium dioxide (IrO_2) were purchased from Shanghai Macklin Biochemical Industrial Co., Ltd. Nickel nitrate hexahydrate ($Ni(NO_3)_2 \cdot 6H_2O$), polyvinylpyrrolidone (PVP, $M_w = 8000$) and dimethyl sulfoxide (DMSO) were purchased from Aladdin Industrial Co., Ltd. All above chemicals and reagents were used as received without further purification. Ni foam (NF, thickness: 0.2 mm) was purchased from Guangzhou Lige Technology Co., Ltd., and cleaned in 6 M HCl, acetone, ethanol, and water, respectively. The deionized water (18.2 MΩ cm) was used throughout the whole experiments.

Preparation of IrO_2@NF electrode

5 mg of IrO_2 with 100 μL of 5 wt% Nafion solution were ultrasonically dispersed in 900 μL of isopropyl alcohol, and the dispersion was drop-cast onto the treated NF electrode to ensure the mass loading of 1.5 mg cm^{-2} for comparison.

Calculation of ECSA

Based on the literature [1], cyclic voltammetry (CV) was carried out in 1 M KOH with 0.5 M urea to probe the electrochemical double-layer capacitance of the various samples at non-Faradic overpotentials to estimate the effective electrode surface areas. Accordingly, a series of CV measurements were performed at various scan rates (20, 40, 60, 80 and 100 mV s^{-1}) in 1.05 – 1.15 V vs. RHE range, and the sweep segments of the measurements were set to 10 to ensure consistency. By plotting the difference in current density (J) between the anodic and cathodic sweeps ($J_{anodic} - J_{cathodic}$) at 1.10 V vs. RHE against the scan rate, a linear trend was observed. The slope of the fitting line was found to be equal-to-twice the geometric double-layer capacitance (C_{dl}), which was proportional to the effective electrode surface area of the materials. Therefore, the electrochemical surface areas of different samples can be compared with one another based on their C_{dl} values. However, it should be noted that this comparison makes sense only when the measurement of materials was carried out under the same condition.

The electrochemically active surface area (ECSA) was calculated from the C_{dl} value following the equations:

$$ECSA = \frac{C_{dl}}{40\ \mu F\ cm^{-2}\ per\ cm_{ECSA}^{2}}$$

Calculation of apparent electrochemical activation energy (E_a)

Given that the UOR can be accelerated by elevating the electrolyte solution, the apparent electrochemical activation energy (E_a) of UOR was determined by the following Arrhenius relationship:

$$\frac{\partial(log\,i_k)}{\partial(1/T)}\Big|\eta = \frac{E_a}{2.3R}$$

where i_k (mA) is the kinetic current of electrodes, T (K) is the solution temperature controlled by a water bath, and R represents the universal gas constant. i_k was selected at 1.5 V (vs RHE) for all materials in 1 M KOH containing 0.5 M urea. The scan rate was 5 mV s^{-1} for polarization curves at various solution temperatures.

DFT calculation

Computational methods

First-principles calculations were performed within the density functional theory framework [2]. The projector-augmented wave (PAW) method [3, 4] and the generalized gradient approximation (GGA) [5] for the exchange-correlation energy functional, as implemented in the Vienna ab initio simulation package (VASP) [6-8] were used. The GGA calculation was performed with the Perdew-Burke-Ernzerhof (PBE) [9] exchange-correlation potential. Considered long-range interaction between molecules/intermediates and surface, Van der Waals interactions were considered using DFT-D3 correlation. A combined supercell slab model was built to simulate the surface of α-NiMoO$_4$ (020), β-NiMoO$_4$ (002) and β-NiMoO$_4$ (400). To avoid effects come from other slabs, a vacuum of 20 Å was added along z direction. The convergence criterion of geometry relaxation was set to 0.01 eV·Å^{-1} in force on each atom. The energy cutoff for plane wave-basis was set to 500 eV. The K points were sampled with 3×3×1 by

Monkhorst-Pack method.

The change in free energy (ΔG) of per reaction step was calculated as following [10]:

$$\Delta G = \Delta E + \Delta ZPE - T \cdot \Delta S + \Delta G_{U} + \Delta G_{pH}$$

Where ΔE is the change of the total reaction energy obtained from DFT calculation, ΔZPE is the change of the zero-point energy, T is the temperature (300K), and ΔS is the change of the entropy. $\Delta G_{U} = -eU$, where U is the potential at the electrode and e is the transferred charge. $\Delta G_{pH} = k_{B} \cdot T \times \ln 10 \times pH$, where k_{B} is the Boltzmann constant and T = 300 K. In this work, the influence of pH was neglected.

Calculation of the surface energies (σ)

The surface energies (σ) are calculated by the following equation [11]:

$$\sigma = \frac{E_{surf} - n \times E_{bulk}}{2S}$$

Where E_{surf} and E_{bulk} are calculated of surface energy and unitcell bulk model energy, respectively. n is the number of atoms in the surface model divided by the number of atoms in the unit cell model. S is the area of the surface model. 2 indicates the two surfaces of the slab model.
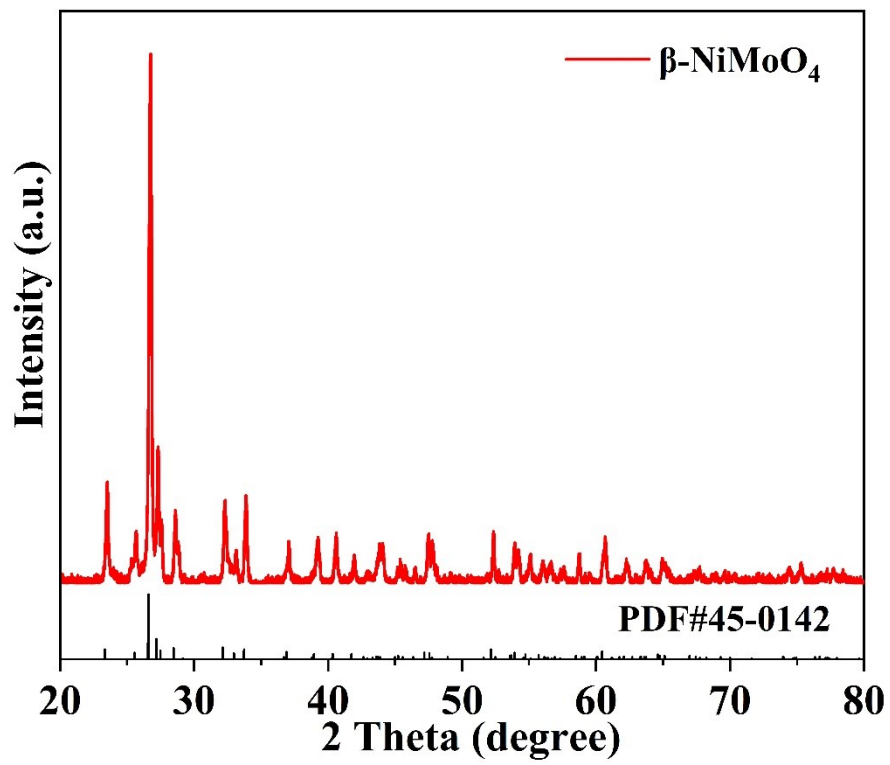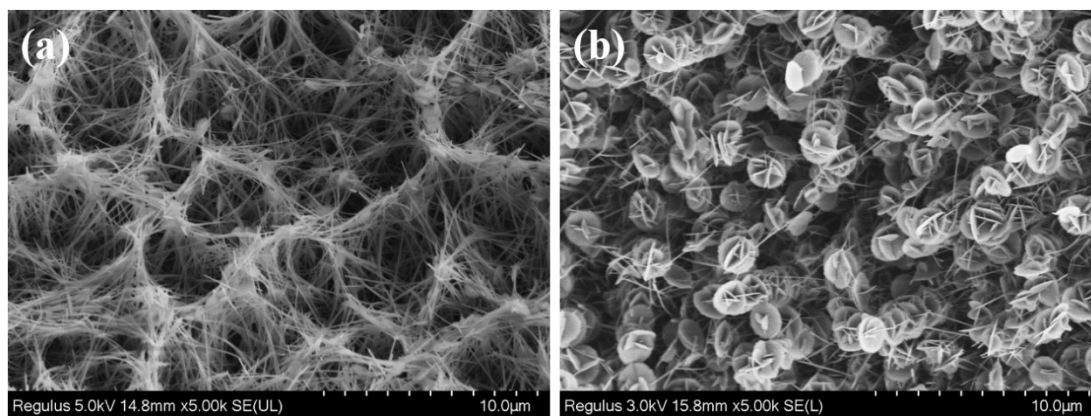
Fig. S1 PXRD pattern of β-NiMoO₄.

Fig. S2 SEM images of α/β-NiMoO$_4$@NF (**a**) without PVP and (**b**) with PVP.

As shown in **Fig. S2**, when PVP is not added to the reaction, the morphology of α/β-NiMoO$_4$@NF is separated from nanorods and nanosheets. Upon adding PVP as the precursor, 2D β-NiMoO$_4$ nanosheets are attached to 1D α-NiMoO$_4$ nanorods array on 3D foam substrate, resulting into the formation of hierarchical α/β-NiMoO$_4$ heterostructure array.
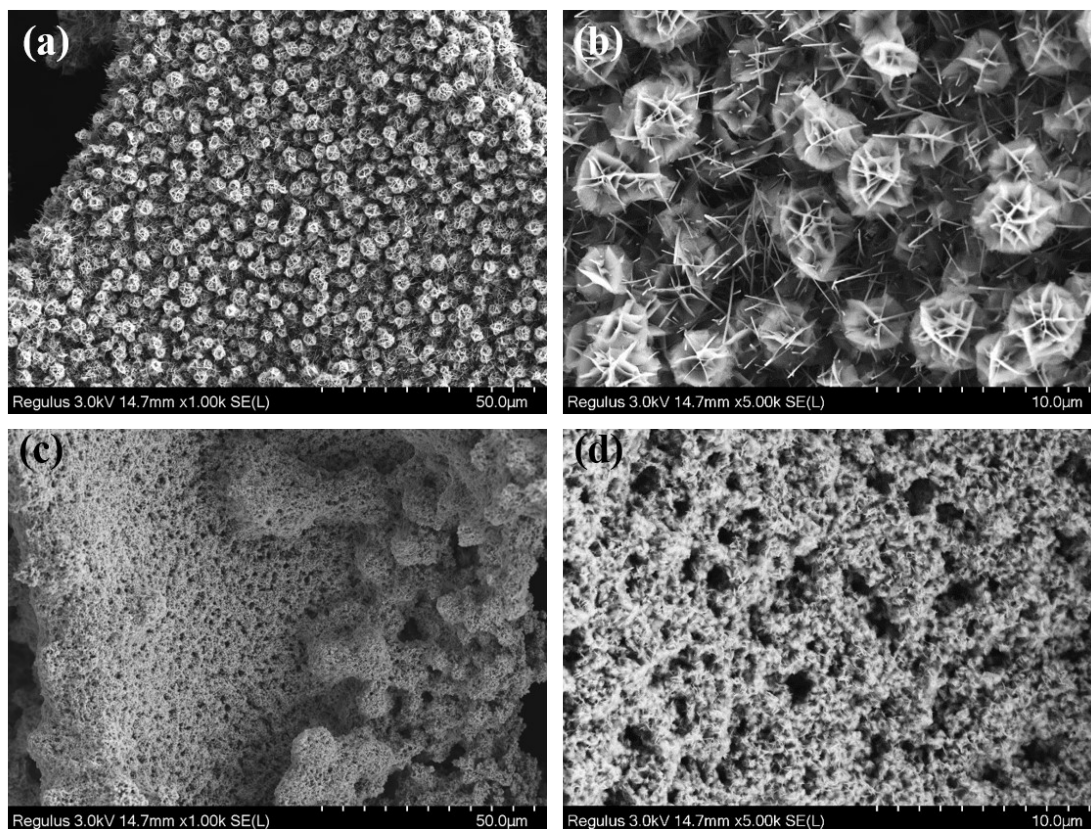
Fig. S3 SEM images of α/β-NiMoO$_4$@NF prepared with different volume ratio of DMSO and H$_2$O under different magnifications. (**a**, **b**) 1:3 and (**c**, **d**) 3:1.
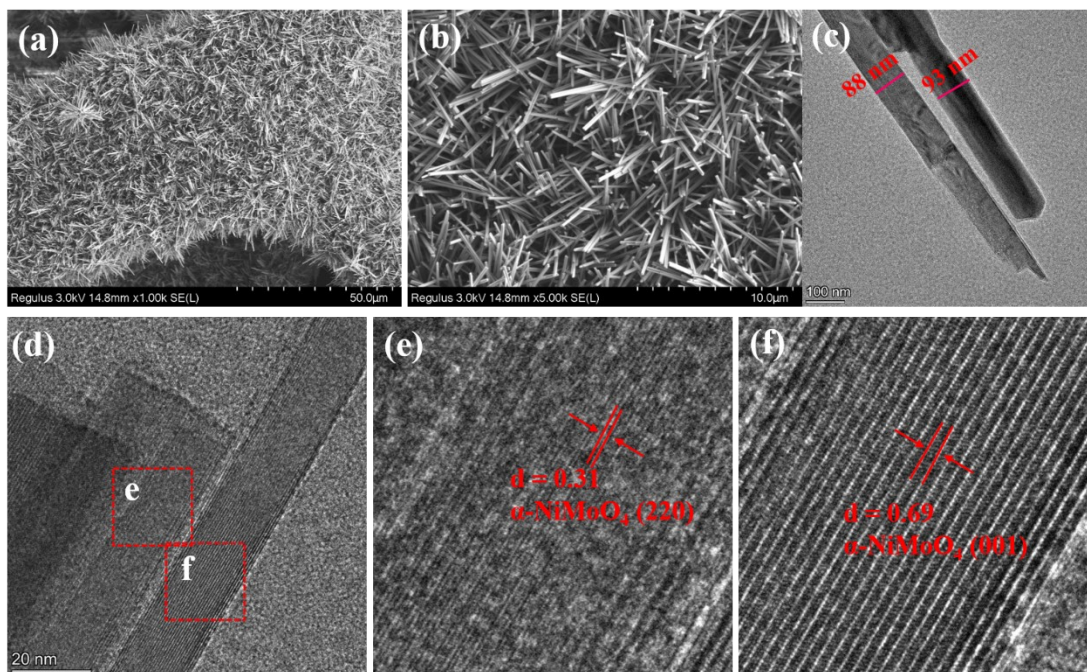
Fig. S4 (**a**, **b**) SEM images of α-NiMoO$_4$@NF at different magnification; (**c**) TEM image and (**d-f**) HRTEM image of α-NiMoO$_4$@NF.

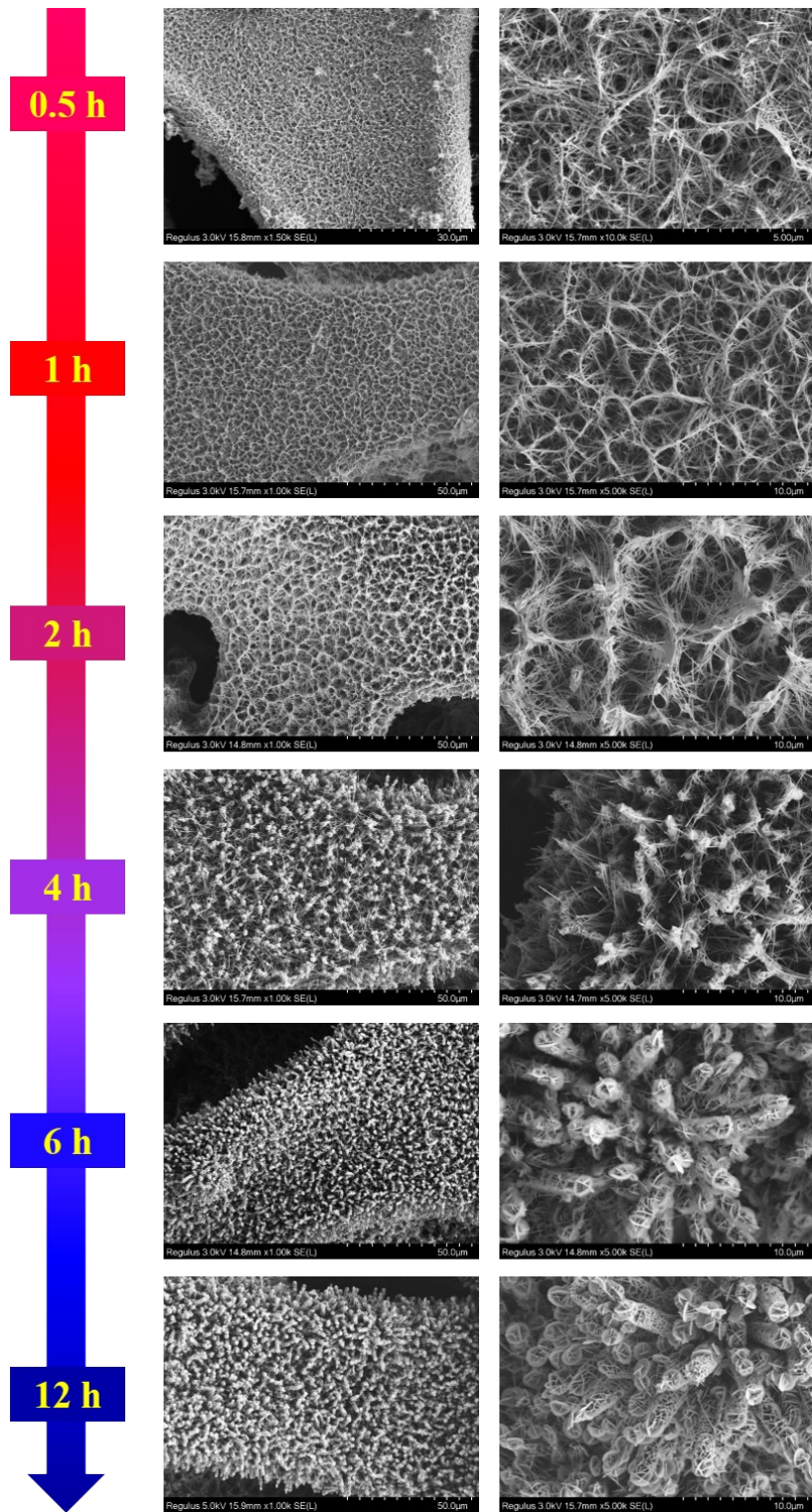**Fig. S5** SEM images of α/β-NiMoO$_4$@NF with different growth time.
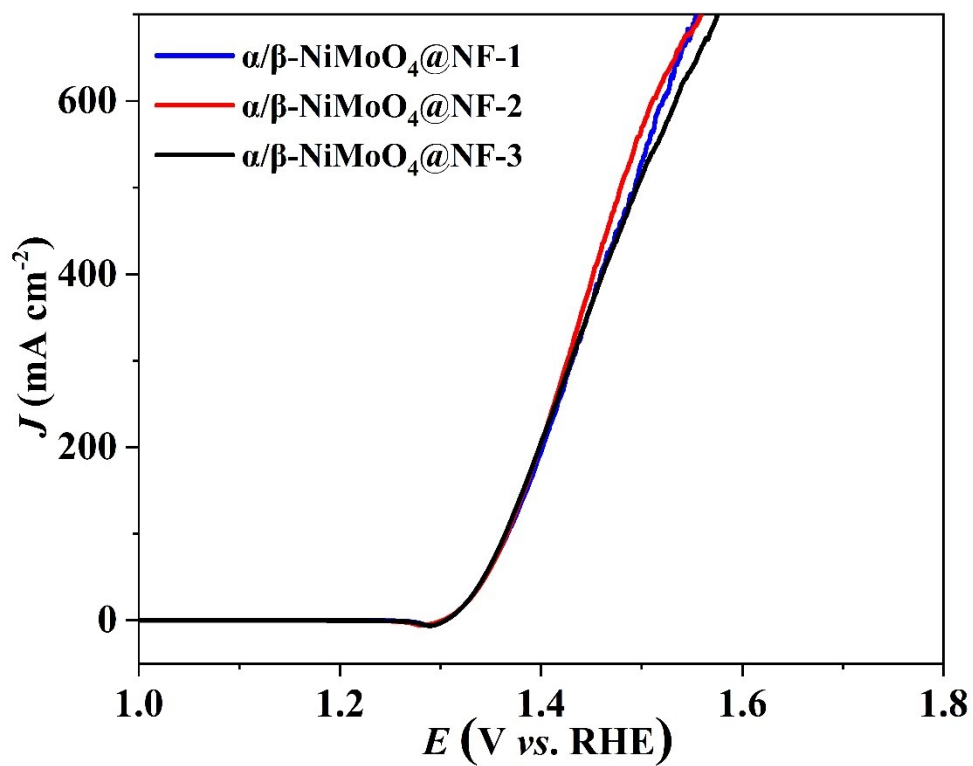
Fig. S6 The LSV curves of α/β-NiMoO₄@NF.
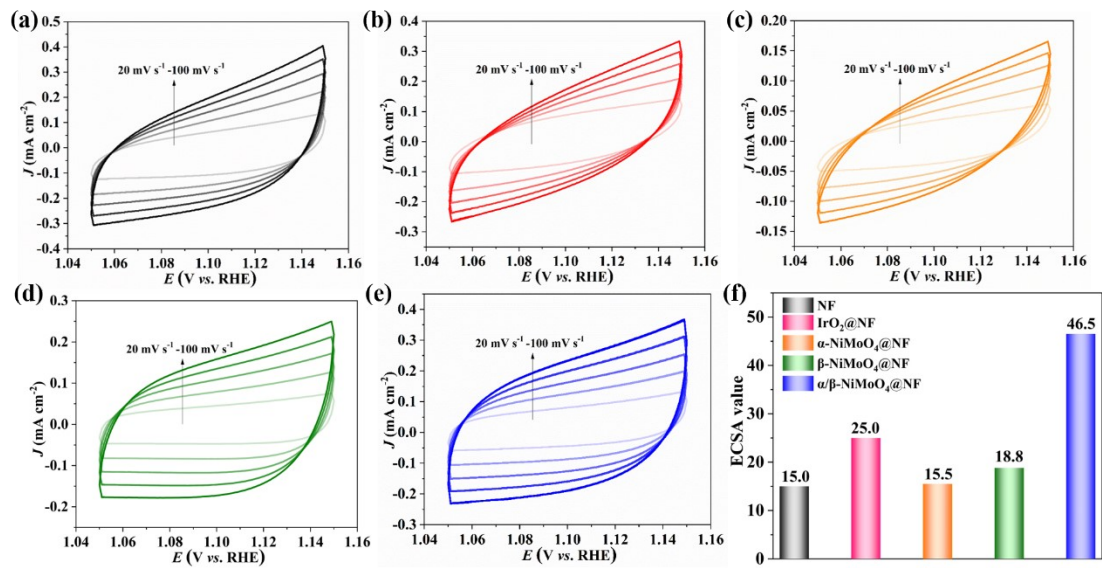
Fig. S7 CV curves of (**a**) NF, (**b**) IrO$_2$@NF, (**c**) α-NiMoO$_4$@NF, (**d**) β-NiMoO$_4$@NF and (**e**) α/β-NiMoO$_4$@NF; (**f**) The ECSA values.
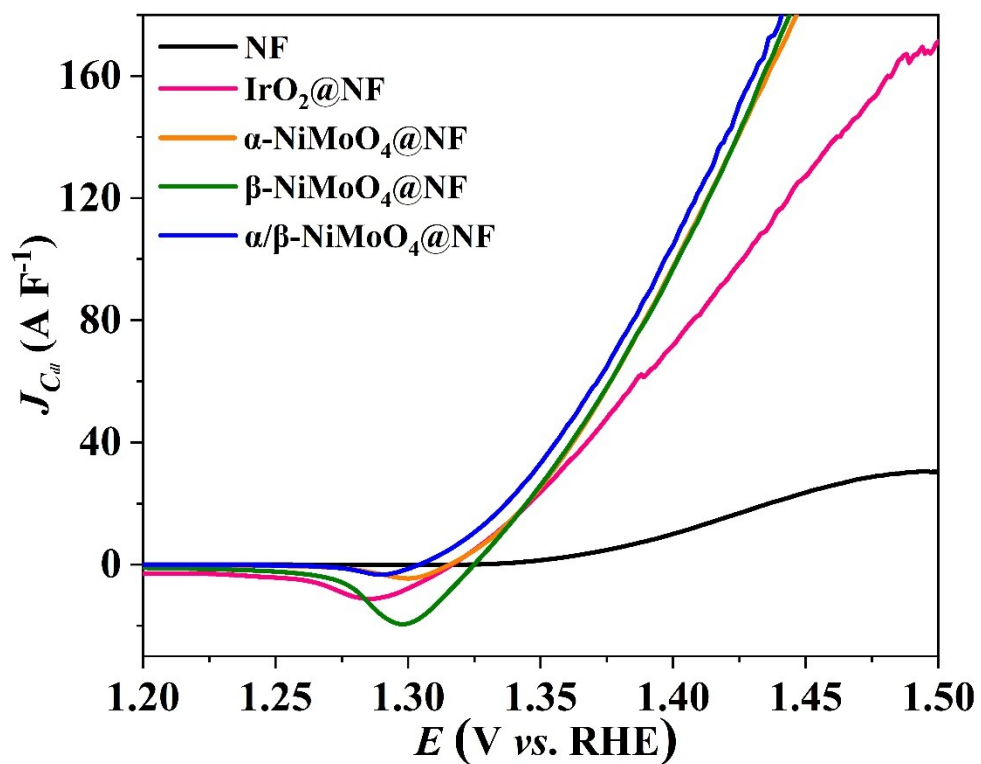
Fig. S8 C_{dl}-normalized LSV curves of NF, IrO$_2$@NF, α-NiMoO$_4$@NF, β-NiMoO$_4$@NF and α/β-NiMoO$_4$@NF.
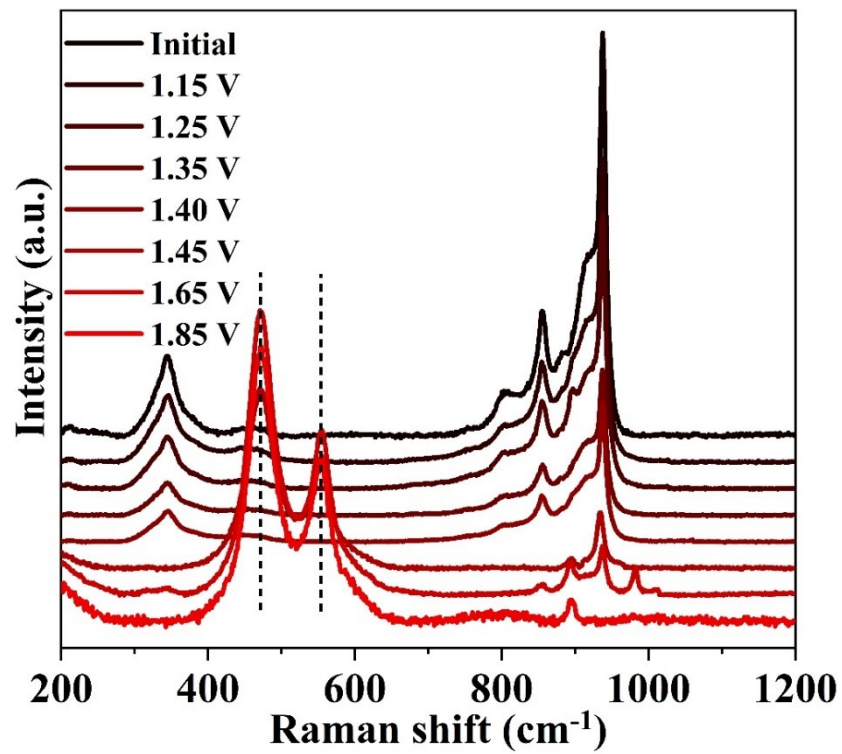
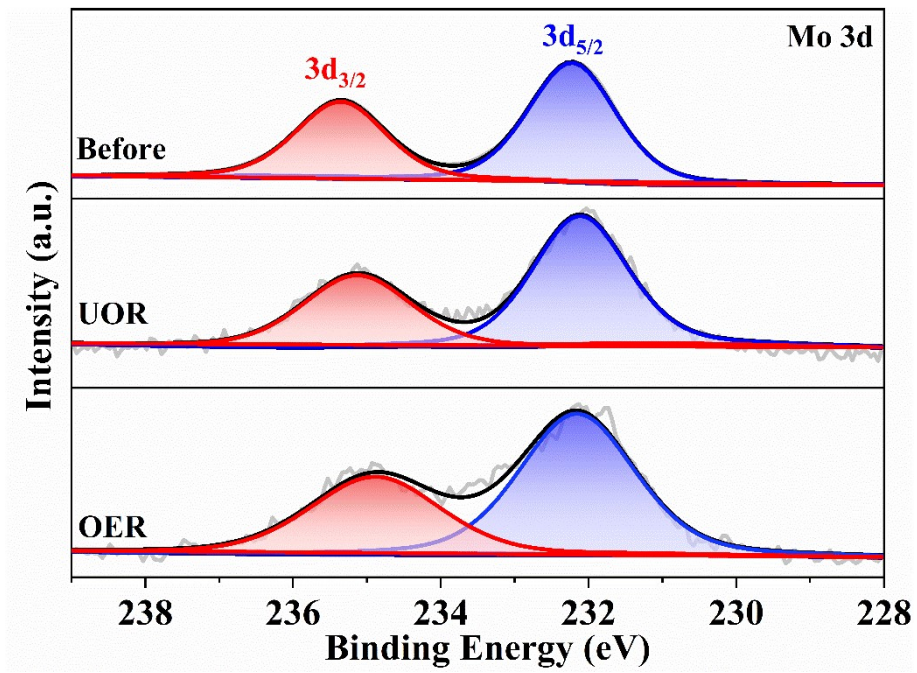**Fig. S9** In-situ Raman spectra of α/β-NiMoO$_4$@NF during OER process test at 25℃.

Fig. S10 Mo 3d XPS spectra for α/β-NiMoO$_4$@NF electrode before and after OER and UOR test.
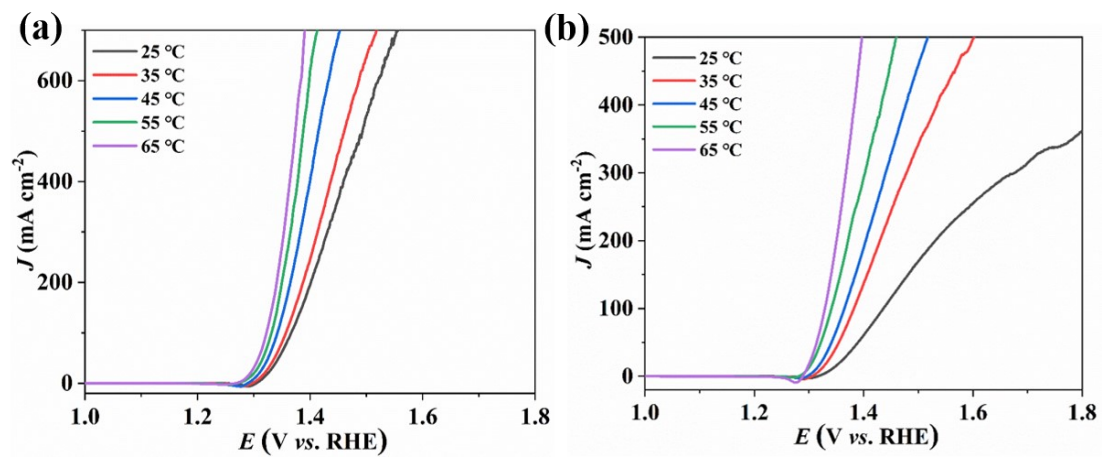
Fig. S11 LSV curves of (**a**) α/β-NiMoO$_4$@NF, (**b**) α-NiMoO$_4$@NF electrode tested at 25-65 ℃.
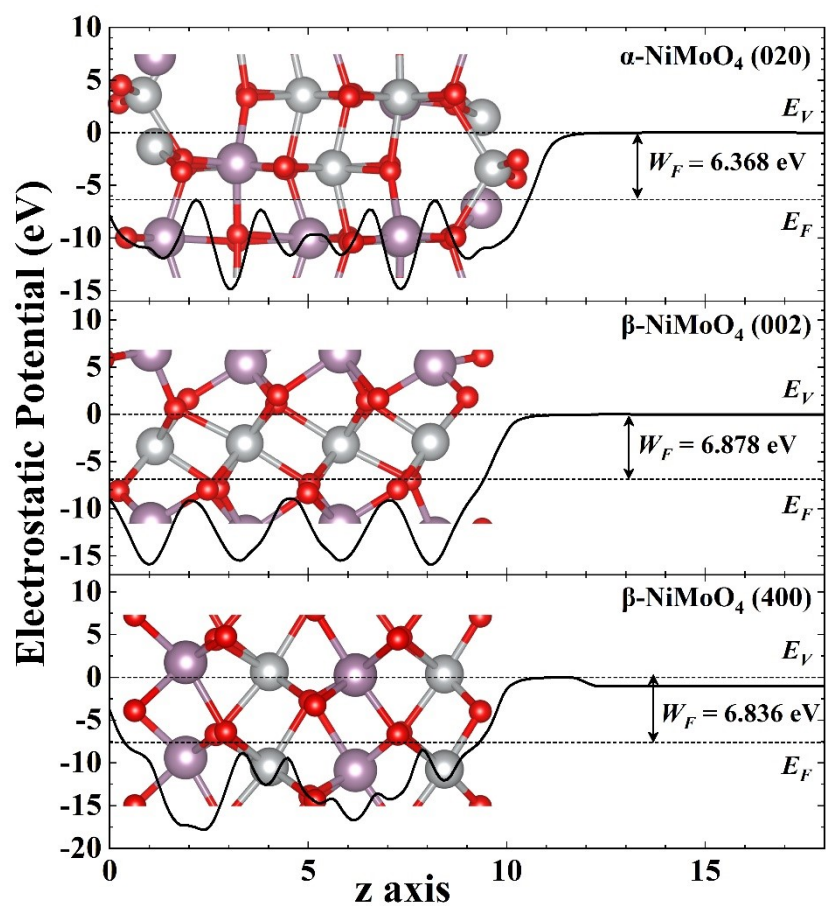
Fig. S12 The electrostatic potentials of α-NiMoO$_4$ (020), β-NiMoO$_4$ (002) and β-NiMoO$_4$ (400) surfaces.
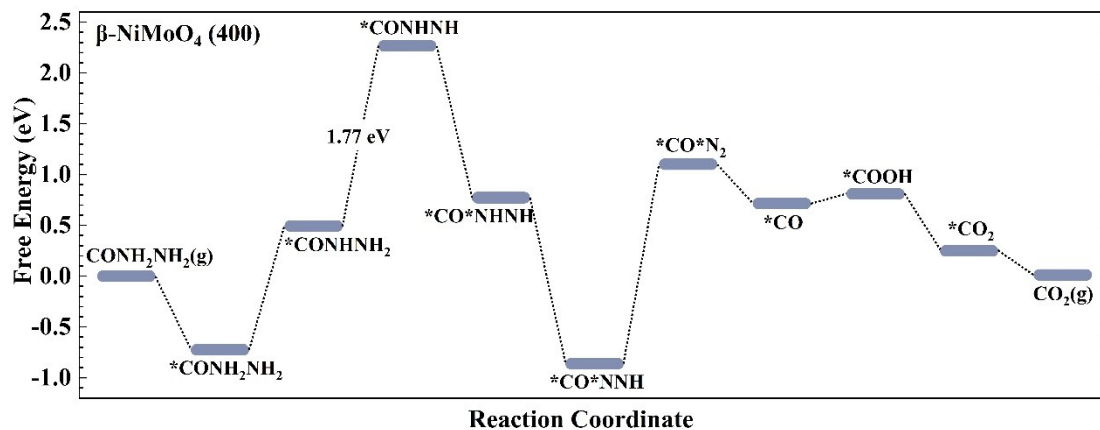
Fig. S13 The Gibbs free energy (ΔG) profiles calculated at the standard conditions along the reaction pathways of UOR on the β-NiMoO$_4$ (400) surface.

Table S1 Summary of the UOR activity of recently reported Ni and Mo-containing oxides electrocatalysts

catalysts	electrolyte	η for UOR@ corresponding j (mV@mA cm^{-2})	Δη for UOR and OER	Ref.
β-NiMoO$_4$	1.0 M KOH+ 0.5 M Urea	250@100	270 mV@ 100 mA cm^{-2}	[12]
r/NiMoO$_4$/NF	1.0 M KOH+ 0.5 M Urea	213@100	380 mV@ 100 mA cm^{-2}	[13]
NF/NiMoO-Ar	1.0 M KOH+ 0.5 M Urea	190@100	210 mV@ 100 mA cm^{-2}	[14]
NiMoO$_3$S/NF	1.0 M KOH+ 0.5 M Urea	110@10	--	[15]
NiS@Ni$_3$S$_2$@ NiMoO$_4$	1.0 M KOH+ 0.5 M Urea	70@10 220@100	250 mV@ 100 mA cm^{-2}	[16]
Ni-Mo nanotube	1.0 M KOH+ 0.1 M Urea	130@10 160@50	210 mV@ 100 mA cm^{-2}	[17]
MS- Ni$_2$P/Ni$_{0.96}$S/NF	1.0 M KOH+ 0.5 M Urea	210@10	220 mV@ 100 mA cm^{-2}	[18]
α-NiMoO$_4$@NF	1.0 M KOH+ 0.5 M Urea	88	--	[19]
α/β-NiMoO$_4$@NF	**1.0 M KOH+ 0.5 M Urea**	**130@100 262@500**	**345 mV@ 100 mA cm^{-2}**	**This work**

Table S2 The value of solution resistances (R_s) and charge transfer resistances (R_{ct})

Surface	$R_s(\Omega)$	$R_{ct}(\Omega)$
α/β-NiMoO$_4$@NF	3.1	3.2
β-NiMoO$_4$@NF	6.0	3.9
α-NiMoO$_4$@NF	3.4	6.8
IrO$_2$@NF	3.3	4.6
NF	3.1	37.3

Table S3 The content of Ni^{2+}, Ni^{3+} and O_v in α/β-NiMoO$_4$@NF before and after UOR

Content	Ni^{2+}	Ni^{3+}	O_v
Before	40.19%	24.5%	34.9%
UOR	39.71%	22.36%	39.7%

References

1. J. F. Xie, S. Li, X. D. Zhang, J. J. Zhang, R. X. Wang, H. Zhang, B. C. Pan and Y. Xie, Atomically-thin molybdenum nitride nanosheets with exposed active surface sites for efficient hydrogen evolution, *Chem. Sci.*, 2014, **5**, 4615-4620.

2. W. Kohn and L. J. Sham, Self-consistent equations including exchange and correlation effects, *Phys. Rev.*, 1965, **140**, A1133-1138.

3. P. E. Blöchl, Projector augmented-wave method, *Phys. Rev. B*, 1994, **50**, 17953-17979.

4. G. Kresse and D. Joubert, From ultrasoft pseudopotentials to the projector augmented-wave method, *Phys. Rev. B*, 1999, **59**, 1758-1775.

5. J. P. Perdew and Y. Wang, Accurate and simple analytic representation of the electron-gas correlation energy, *Phys. Rev. B*, 1992, **45**, 13244-13249.

6. G. Kresse and J. Hafner, Ab initio molecular dynamics for liquid metals, *Phys. Rev. B*, 1993, **47**, 558-561.

7. G. Kresse and J. Furthmüller, Efficient iterative schemes for ab initio total-energy calculations using a plane-wave basis set, *Phys. Rev. B*, 1996, **54**, 11169-11186.

8. G. Kresse and J. Furthmüller, Efficiency of ab-initio total energy calculations for metals and semiconductors using a plane-wave basis set, *Comput. Mater. Sci.*, 1996, **6**, 15-50.

9. J. P. Perdew, K. Burke and M. Ernzerhof, Generalized gradient approximation made simple, *Phys. Rev. Lett.*, 1996, **77**, 3865-3868.

10. J. K. Nørskov, J. Rossmeisl, A. Logadottir, L. Lindqvist, J. R. Kitchin, T. Bligaard and H. Jonsson, Origin of the overpotential for oxygen reduction at a fuel-cell cathode, *J. Phys. Chem. B*, 2004, **108**, 17886-17892.

11. X. Tian, T. Wang, L. Fan, Y. Wang, H. Lu and Y. Mu, A DFT based method for calculating the surface energies of asymmetric MoP facets, *Appl. Sur. Sci.*, 2018, **427**, 357-362.

12. G. Wu, W. Chen, X. Zheng, D. He, Y. Luo, X. Wang, J. Yang, Y. Wu, W. Yan, Z. Zhuang, X. Hong and Y. Li, Hierarchical Fe-doped NiO_x nanotubes assembled from ultrathin nanosheets containing trivalent nickel for oxygen evolution reaction, *Nano Energy*, 2017, **38**, 167-174.

13. Z.-Y. Yu, C.-C. Lang, M.-R. Gao, Y. Chen, Q.-Q. Fu, Y. Duan and S.-H. Yu, Ni–Mo–O nanorod-derived composite catalysts for efficient alkaline water-to-hydrogen conversion via urea electrolysis, *Energy Environ. Sci.*, 2018, **11**, 1890-1897.

14. Y. Yang, S. T. Wang, C. H. Jiang, Q. C. Lu, Z. L. Tang and X. Wang, Controlled synthesis of hollow Co–Mo mixed oxide nanostructures and their electrocatalytic and lithium storage properties, *Chem. Mater.*, 2016, **28**, 2417-2423.

15. L. An, J. Feng, Y. Zhang, R. Wang, H. Liu, G. C. Wang, F. Cheng and P. Xi, Epitaxial Heterogeneous Interfaces on $N-NiMoO_4/NiS_2$ Nanowires/Nanosheets to Boost Hydrogen and Oxygen Production for Overall Water Splitting, *Adv. Funct.*, 2019, **29**, 1805298.

16. Z. Zhang, X. Ma and J. Tang, Porous $NiMoO_{4–x}/MoO_2$ hybrids as highly effective electrocatalysts for the water splitting reaction, *J. Mater. Chem. A*, 2018, **6**, 12361-12369.

17. X. D. Yan, L. H. Tian, S. Atkins, Y. Liu, J. Murowchick and X. B. Chen, Converting $CoMoO_4$ into CoO/MoO_x for overall water splitting by hydrogenation, *ACS Sustainable Chem. Eng.*, 2016, **4**, 3743-3749.

18. M. Yang, Y. Jiang, M. Qu, Y. Qin, Y. Wang, W. Shen, R. He, W. Su and M. Li, Strong electronic couple engineering of transition metal phosphides-oxides heterostructures as

multifunctional electrocatalyst for hydrogen production, *Appl. Catal. B-Environ.*, 2020, **269**, 118803.

19. Y. Li, H. Xu, H. Huang, C. Wang, L. Gao and T. Ma, One-dimensional MoO_2–$Co_2Mo_3O_8$@C nanorods: a novel and highly efficient oxygen evolution reaction catalyst derived from metal–organic framework composites, *Chem. Commun.*, 2018, **54**, 2739-2742.